ASTRONOMY & ASTROPHYSICS
SUPPLEMENT SERIES

Astron. Astrophys. Suppl. Ser. **109,** 109-123 (1995)

CEPAM: a code for modeling the interiors of giant planets

T. Guillot and P. Morel

Cassini, URA CNRS 1362 and GDR CNRS G 131, Observatoire de la Côte d'Azur, BP. 229, F-06304 Nice Cedex 4, France

Received May 17; accepted August 3, 1994

Abstract. — The aim of this paper is to describe the numerical techniques used in the code CEPAM, developed to study the internal structure of giant planets. The main originality of CEPAM is the solution of the two point boundary value problem of the quasi-static equilibrium by a collocation implicit method based on piecewise polynomial approximations projected on a B-spline basis. An automatic mesh refinement is designed to adjust the location of the grid points depending on the variation in the unknowns. Moreover, a grid point can be adjusted at any determined position. This allows an exact treatment of the problem, even when the first derivatives of the integration variables (M, R, P, T, L) are discontinuous. A robust optimization method allows the calculation of models matching the observed equatorial radius and gravitational moments. The numerical accuracy of the models calculated is found to be satisfactory even with a small number of mesh points (the relative accuracy is better than 10^{-5} on all the variables with 100 mesh points). The whole precision of models of giant planets is limited by the accuracy of physical data.

Key words: methods: numerical — planets: individual; Jupiter; Neptune; Saturn; Uranus

1. Introduction

The giant planets are natural laboratories for the study of the behavior of matter at high pressures and temperatures, in a region that can barely be reached in laboratory and where non-ideal effects are preponderant. They provide also very good tests for the models of formation and evolution of our solar system. Thus, they became the focus of many studies since the pioneering work of Jeffreys (1923).

The observations of giant planets have led to more and more accurate constraints, particularly since *Pioneer* and *Voyager* measurements. The accuracy of the numerical models of internal structure of these planets should therefore be consistent with the precision reached by the observations, though the uncertainties on physical theories of matter at high density, especially in the region $\rho \approx 1\,\mathrm{g.cm^{-3}}$, are, at the present time, still large and do not seem to require a large exactness of the models.

A first way to improve the numerical precision of a model is, evidently, to increase the number of grid points, a second way is to use numerical algorithms of high order. (In fact, for reaching a given accuracy, there is a compromise between the number of grid points and the order of the scheme to be employed.)

Up to now the models of giant planets' interiors have been computed with explicit methods (Hubbard & Marley 1989; Chabrier et al. 1992). This method has given good results and could eventually be implemented with algorithms of higher order. However it has only been designed for the study of adiabatic models, i.e. models for which the temperature gradient can be directly determined by the equation of state. With the possibility of a non-adiabatic structure of the interior of giant planets, pointed out by Guillot et al. (1994a), a better method seems to treat the more complicated quasi-static problem as an implicit two point boundary value problem, as it is done for stellar interior modeling since the work of Henyey et al. (1959). Robust, flexible and accurate algorithms can then be obtained. This technique is employed in the numerical code CEPAM[1], which has been adapted from the stellar code CESAM (Morel 1989). CEPAM has been used for the accurate calculation of models of Jupiter and Saturn (Guillot et al. 1994b; Mosser et al. 1994).

Another feature of CEPAM is its modularity: all the physical inputs (equation of state, opacity,... etc.) are computed only from external routines. Hence, it is possible to adapt a specific part of the physics without any other internal modification in the code.

The basis of CEPAM is a numerical technique for the integration of the two point boundary value problem derived by de Boor (1978). The basic idea is to write the unknown functions as piecewise polynomials of a given order, and project them on their B-spline basis (de Boor

Send offprint requests to: T. Guillot (guillot@obs-nice.fr)

[1] Code d'Evolution Planétaire Adaptatif et Modulaire.

1978; Schumaker 1981), which is, for the calculations, much more convenient than the canonical basis of the linear space of piecewise polynomials. The main advantages are, essentially, efficient and stable computations and a very large flexibility. Moreover, discontinuities are treatable without significant modifications of the algorithms. Finally, with a very convenient basis of B-splines, the integration is of Gaussian type, which improves the order of the scheme: the so-called "superconvergence". Its main disadvantage is a consequence of the non trivial and not familiar algebra of B-splines: the algorithms are much more difficult to read than those with finite differences.

We recall in Sect. 2 the physical bases motivating a numerical study: we formulate the differential problem of quasi-static equilibrium and discuss the boundary conditions determined from the observations as well as the qualitative internal structure of giant planets.

In Sect. 3, we describe the method used to solve the two point boundary value problem. In this paper we focus on the determination of *static* models. The evolution problem, although treatable with this code, will only be mentioned in this paper but not reported. Section 4 is devoted to comparisons of the models obtained. We discuss there the internal relative accuracy of the solution that can be expected with a reasonable number of meshes.

2. Physical inputs

2.1. *Structure of the giant planets*

A qualitative view of the interior of giant planets is presented in Fig. 1. The most striking features are that, contrary to a star like the Sun, the four giant planets, first, are too cold to ignite thermonuclear reactions and, second, are supposed to possess a central dense core, whose composition (and density) is totally different from that of the envelope which is mainly composed of hydrogen and helium.

This is important as, first, the equation of state (EOS) used in the envelope is different from the EOS valid in the core (Hubbard & Marley 1989; Chabrier et al. 1992) and, second, there is a jump of the density across the transition envelope/core.

This core is, itself, possibly formed by a central part of "rocks" with a surrounding layer of "ices". Therefore, the density therein can also be discontinuous.

Moreover, the pressures involved inside Jupiter and Saturn are sufficiently high to pressure-ionize hydrogen. As pointed out by Saumon & Chabrier (1991, 1992), this transition between molecular and metallic hydrogen (Plasma Phase Transition or PPT) should be first-order. Hence, a discontinuity of the density across this transition has to be considered too.

The other important point is that the giant planets rotate rapidly (typically in about 10 hours). However, as reviewed by Zharkov & Trubitsyn (1978), this problem can be handled without changing the form of the equations for quasi-static equilibrium. With a development of the radius in Legendre polynomials, one finds that a term V_ω added to the hydrostatic equation, is sufficient to take into account the rotation. The radius, R, then represents the *mean radius*.

A consequence of the rotation is that the external gravitational field no longer possesses spherical symmetry. The departure from this symmetry depends on the rotation velocity and on the density profile and can be determined by studying the movement of a close satellite. Thus, some of the gravitational moments of the planet J_{2n}, $(n = 1, 2, 3)$, are known and constitute accurate constraints for interior models (see Appendix).

2.2. *Equations for the quasi-static equilibrium*

With M, the mass, as independent (lagrangian) variable, the internal structure of giant planets is governed by the following system of differential equations:

$$\begin{cases} \dfrac{\partial P}{\partial M} = -\dfrac{GM}{4\pi R^4} + V_\omega \\ \dfrac{\partial T}{\partial M} = \left(\dfrac{\partial P}{\partial M}\right)\dfrac{T}{P}\nabla \\ \dfrac{\partial R}{\partial M} = \dfrac{1}{4\pi R^2 \rho} \\ \dfrac{\partial L}{\partial M} = \mathcal{E} - T\dfrac{\partial S}{\partial t}, \end{cases} \tag{1}$$

where the following classical symbols have been employed: R: mean radius, P: pressure, ρ: density, G: gravitational constant, T: temperature, $\nabla \equiv \partial \ln T / \partial \ln P$: gradient, L: luminosity, $\mathcal{E}$: energy production rate due to any source of energy, S: specific entropy, t: time, $4\pi R^2 V_\omega$: centrifugal acceleration due to the angular velocity ω.

The rotation term V_ω can be developed as (see Zharkov & Trubitsyn 1978):

$$V_\omega = \frac{\omega^2}{6\pi R} + \frac{GM_{\rm tot}}{4\pi R_{\rm tot}^3 R}\varphi_\omega, \tag{2}$$

where $M_{\rm tot}$ and $R_{\rm tot}$ are the total mass and radius of the planet, and φ_ω corresponds to the undimensioned rotation perturbation at high order (see Appendix).

2.2.1. Internal boundary conditions

The boundary conditions at the center, $M = 0$, can trivially be written as:

$$R = 0, \quad L = 0.$$

However, as we will see, it is more convenient to separate the integration of the core and the integration of the envelope. Hence these internal boundary conditions will only be used for the integration of the core.

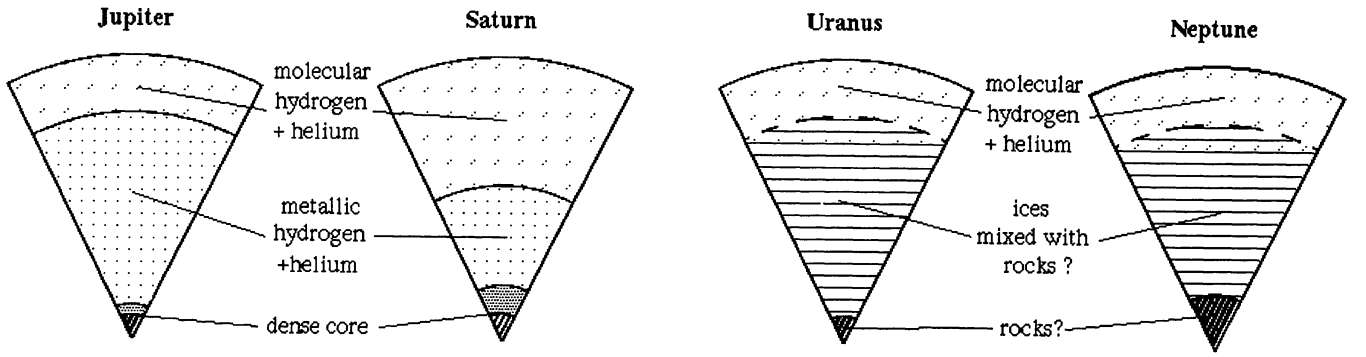

Fig. 1. The interior of the four giant planets, according to "conventional wisdom"

2.2.2. External boundary conditions

The measurements inferred from *Voyager* data yield an accurate determination of the external conditions in the four giant planets. These conditions are usually fixed at the external $P_{\rm ext}$=1 bar pressure level, for which the corresponding mass $M_{\rm ext}$ and luminosity $L_{\rm ext}$ are nearly equal to the total mass $M_{\rm tot}$ and luminosity $L_{\rm tot}$ of the planet. The equatorial radius $R_{\rm eq}$ as well as the temperature $T_{\rm ext}$ have been accurately measured for this pressure level.

These measurements show that below this 1 bar level the temperature profile is adiabatic (Lindal 1981) and that the presence of clouds provides a semi-infinite ($\tau > 100$) optical depth (Bézard et al. 1983). Thus, the diffusion approximation, which is only valid in the optically thick medium, is a very good assumption in the whole domain studied. This is important since the gradient ∇ in Eq. (1) is calculated within the classical mixing length formalism and using Rosseland mean opacities (see e.g. Kippenhahn & Weigert 1991).

Along the evolution a relation between the 1 bar temperature and the intrinsic luminosity of the planet can be deduced from the calculations of Graboske et al. (1975). Then the external boundary remains fixed at the 1 bar level, but the conditions are functions of the time. Hence, at $M = M_{\rm tot}$, we set:

$$T = T_{\rm ext}(L(M_{\rm ext}), t), \quad P = 1\,\text{bar}.$$

2.3. *Evolution*

Due to the fact that their interiors are relatively cold, no thermonuclear reactions occur inside the giant planets. It could be assumed that the problem of their evolution is governed only by their contraction and cooling. However, two other phenomena may have a significant effect on the energy generation. First, during the evolution, as the planet was hotter and is cooling, the PPT has moved from the exterior to the interior. Some energy has been released due to the latent heat produced by the transformation of molecular to metallic hydrogen. However, this occurs early in the evolution (about 10^8 yrs after the formation) and seems to have only a small influence on the history of Jupiter and Saturn (Saumon et al. 1992).

Second, if the inner temperature is sufficiently low, a phase *separation* between hydrogen and helium can occur (Stevenson & Salpeter 1977). The gravitational energy released by helium-rich droplets falling toward the core should be significant and affects the evolution. This is indeed a probable explanation for the high intrinsic luminosity of Saturn.

3. Solving the two point boundary value problem

3.1. *Separation of the integration: core and envelope*

As previously mentioned, giant planets are thought to consist of a dense central core surrounded by a hydrogen-helium envelope, whose structures and compositions are very different. Therefore, two (or more) EOS are used for the integration of the core, and of the envelope, respectively. Moreover, the masses of the cores of Jupiter and Saturn appear to be small compared to the total masses of the planets. Therefore their thermal properties have little influence on the planets heat content and one can assume that the cores are isothermal. This simplifies considerably the equations and, for the core, the system (1) can simply be written as:

$$\begin{cases} \dfrac{\partial P}{\partial M} = -\dfrac{GM}{4\pi R^4} + V_\omega, \\ \dfrac{\partial R}{\partial M} = \dfrac{1}{4\pi R^2 \rho}. \end{cases} \tag{3}$$

Attempts have been made to solve simultaneously Eq. (3), for the core and Eq. (1), for the envelope, but the discontinuous properties of the two EOSs tend to destabilize the problem. A good method is therefore to integrate separately, and in turn, the core and the envelope until convergence. The following boundary conditions, which take into account the observed quantities, are used:

$$\text{Envelope} : \begin{cases} M = M_{\rm ext} : & P = P_{\rm ext},\ T = T_{\rm ext}, \\ M = M_{\rm core} : & R = R_{\rm core},\ L = L_{\rm core}. \end{cases} \tag{4}$$

$$\text{Core}: \begin{cases} M = M_{\rm core}: & P = P_{\rm envelope}, \\ M = 0: & R = 0. \end{cases} \quad (5)$$

$L_{\rm core}$ is the core luminosity, $M_{\rm core}$ and $R_{\rm core}$ are the mass and radius of the core and $P_{\rm envelope}$ is the pressure at the bottom of the envelope.$P_{\rm envelope}$ and $R_{\rm core}$ result from the integration of the envelope, and of the core, respectively.

When considering static models, $L_{\rm core}$ is set to $L_{\rm ext}$, the observed intrinsic luminosity. Moreover, the value of L is assumed to be constant throughout the planet. As discussed by Guillot et al. (1994b) this is a good approximation since we only consider radiative zones located in the outermost layers of the planet where the luminosity is constant.

When dealing with planetary evolution, $L_{\rm core}$ will be more properly set to a small, but finite, value, typically the value of the radioactivity of a mass of chondrites equal to the mass of the rocky core.

The structure of the core is solved with the method of integration employed for the envelope but without using mesh refinement, as described hereafter. Hence we integrate Eq. (3) directly, using the mass as independent variable. This is possible because the integration of its structure is quite straightforward and does not require special care. A transition between a "rocky" core and an "icy" core can be included in our calculations. This transition yields a discontinuity of the density. However a distribution function with one mesh located exactly at the transition can be easily found since this transition is always set for a given mass in planetary models. Therefore, the spline/collocation algorithms, described hereafter, allow one to obtain a solution with the required accuracy in the whole core.

The method of numerical integration of the core being a simplified variant of the method used for the envelope, it will not be developed any further.

3.2. *Variables used for the numerical integration of the envelope*

The system of Eq. (1) presents a singularity at the center. This is not a problem for CEPAM (the differential equations are not calculated at the mesh points), yet, a set of variables borrowed from studies of the stars (Eggleton 1971; Morel 1989) appears to be more efficient and avoids this singularity. Thus, the following variables are used in the calculation:

$$\xi = \ln P,\ \eta = \ln T,\ \mu = 1 - \left(\frac{M}{M_{\rm tot}}\right)^{\frac{2}{3}},\ \zeta = \left(\frac{R}{R_{\rm tot}}\right)^2,$$
$$\lambda = \left(\frac{L}{L_{\rm tot}}\right)^{\frac{2}{3}}. \quad (6)$$

With this set of new variables Eq. (1) can be written as:

$$\begin{cases} \dfrac{\partial \xi}{\partial \mu} = \dfrac{e^{-\xi}}{4\pi}\left\{\dfrac{3G}{2}\dfrac{M_{\rm tot}^2}{R_{\rm tot}^4}\left[\left(\dfrac{1-\mu}{\zeta}\right)^{3/2} - \varphi_\omega\right] - \omega^2\right\} \times \\ \qquad \times \left(\dfrac{1-\mu}{\zeta}\right)^{1/2}, \\ \dfrac{\partial \eta}{\partial \mu} = \dfrac{\partial \xi}{\partial \mu}\nabla, \\ \dfrac{\partial \zeta}{\partial \mu} = -\dfrac{3}{4\pi}\dfrac{M_{\rm tot}}{R_{\rm tot}^3}\dfrac{1}{\rho}\left(\dfrac{1-\mu}{\zeta}\right)^{1/2}, \\ \dfrac{\partial \lambda}{\partial \mu} = -\dfrac{M_{\rm tot}}{L_{\rm tot}}\left(\dfrac{1-\mu}{\lambda}\right)^{1/2}\left[\mathcal{E} - T\left(\dfrac{\partial S}{\partial t}\right)_\mu\right]. \end{cases} \quad (7)$$

It is easily shown that both $(1-\mu)/\zeta$ and $(1-\mu)/\lambda$ have no singularity throughout the whole planet. One notes that φ_ω has no singularity either.

3.3. *The mesh refinement: an automated allocation of grid points*

Planetary models are often calculated with equidistant meshes in radius. This method, although probably the most simple, is not very efficient since regions where the gradients of the unknowns are important are treated in the same way as regions where almost no variation occurs. To illustrate this problem, one can look at the variations of the pressure scale height $H_{\rm p}$=dr/dln$P$, which is larger than 10^9 cm in inner regions and about 10^6 cm near the surface of Jupiter and Saturn. Therefore, it is obvious that an accurate treatment of the problem will require more points near the surface than near the center of the planet.

In CEPAM, a grid of points is calculated, with more points in regions where the gradients of the unknowns are important. This is obtained by an automatic mesh refinement.

The most common method for grid refinement consists, on need, by adding or subtracting mesh points; though very simple in its principle, this obvious method is, in fact, difficult to be properly fixed in practice.

With the automatic grid refinement used in CEPAM the number n of mesh points is fixed at once and their location is made by fulfilling the condition that, at a fixed time, the jump of a strictly monotonous "distribution function" $Q(\mu, t)$, is a constant from a grid point to the next (see Eggleton 1971; Press et al. 1986, Sect. 16.5). At each time t, one looks for a distribution of the grid points $\mu_i, i = 1, \ldots, n$ in such a way that:

$$Q(\mu_{i+1}, t) - Q(\mu_i, t) = Cte(t), \quad i = 1, \ldots, n-1. \quad (8)$$

There is a large choice for the distribution function $Q(\mu, t)$; it results from the feeling one has, a priori, of the behavior of the solution. For each value t of the time, one

defines a function subscript[2] $q(\mu,t)$ mapping $[1,\mu_{\rm core}]$ on $[1,n]\subset\mathbf{N}$. We introduce the derivative of Q with respect to q,

$$\psi(t)\equiv\left(\frac{\partial Q}{\partial q}\right)_t. \tag{9}$$

Eq. (8) then becomes:

$$\left(\frac{\partial\psi}{\partial q}\right)_t=0. \tag{10}$$

Note that Q is a linear function of q as soon as the Eqs. (9) and (10) are fulfilled. The change of variables $\mu\rightarrow q(\mu,t)$ gives:

$$\psi(t)=\theta\left(\frac{\partial\mu}{\partial q}\right)_t, \tag{11}$$

where

$$\theta(\mu,t)\equiv(\partial Q/\partial\mu)_t \tag{12}$$

can be derived from the analytic form of $Q(\mu,t)$ and from Eq. (1).

Thus, compared to Eq. (1), there are two more unknowns: $\psi(t)$ and $\mu(q,t)$; they fulfill a system of differential equations of first order with boundary conditions:

$$\left(\frac{\partial\mu}{\partial q}\right)_t=\frac{\psi}{\theta},\qquad\left(\frac{\partial\psi}{\partial q}\right)_t=0,\ \text{with}\ \begin{cases}q=1,\ \mu=0\\ q=n,\ \mu=\mu_{\rm core}\end{cases} \tag{13}$$

These equations are added to Eq. (1) written with respect to q and t. The set of equations to be solved on the *equidistant* grid $q_i=i$, $i=1,\ldots,n$ is therefore:

$$\begin{cases}\dfrac{\partial\xi}{\partial q}=\dfrac{e^{-\xi}}{4\pi}\left\{\dfrac{3G}{2}\dfrac{M_{\rm tot}^2}{R_{\rm tot}^4}\left[\left(\dfrac{1-\mu}{\zeta}\right)^{3/2}-\varphi_\omega\right]-\omega^2\right\}\times\\ \qquad\times\left(\dfrac{1-\mu}{\zeta}\right)^{1/2}\dfrac{\psi}{\theta},\\ \dfrac{\partial\eta}{\partial q}=\dfrac{\partial\xi}{\partial q}\nabla,\\ \dfrac{\partial\zeta}{\partial q}=-\dfrac{3}{4\pi}\dfrac{M_{\rm tot}}{R_{\rm tot}^3}\dfrac{1}{\rho}\left(\dfrac{1-\mu}{\zeta}\right)^{1/2}\dfrac{\psi}{\theta},\\ \dfrac{\partial\lambda}{\partial q}=-\dfrac{M_{\rm tot}}{L_{\rm tot}}\left(\dfrac{1-\mu}{\lambda}\right)^{1/2}\left[\mathcal{E}-T\left(\dfrac{\partial S}{\partial t}\right)_\mu\right]\dfrac{\psi}{\theta},\\ \dfrac{\partial\mu}{\partial q}=\dfrac{\psi}{\theta},\\ \dfrac{\partial\psi}{\partial q}=0.\end{cases} \tag{14}$$

For the envelope the boundary conditions (4) are written:

$$\begin{cases}\mu(1,t)=0,\ \xi(1,t)=\xi_{\rm ext}(t),\ \eta(1,t)=\eta_{\rm ext}(t),\\ \mu(n,t)=\mu_{\rm core},\ \zeta(n,t)=\zeta_{\rm core},\ \lambda(n,t)=\lambda_{\rm core}(t).\end{cases} \tag{15}$$

[2] in CEPAM the shell with the subscript 1 (resp. n) corresponds to the outer (resp. to the center). Therefore, μ=0 when q=1 and $\mu=\mu_{\rm core}$ for q=n.

For the core, similar relationships can be inferred from Eq. (5).

Since the set of non linear differential Eqs. (14) is solved by an iterative process, the initial value for the distribution function can be derived directly from the initial model.

On the other hand, the differentiation with respect to the grid function q yields much better accuracy than the same differentiation with respect to the mass μ: between two meshes $\Delta\mu$ can become very small, and then imprecise, whereas Δq is, by definition, constant and equal to unity.

Let us introduce the following notation which will simplify the discussion:

$$\begin{aligned}&y_{i,1}\equiv\xi(q_i),\ y_{i,2}\equiv\eta(q_i),\ y_{i,3}\equiv\zeta(q_i),\ y_{i,4}\equiv\lambda(q_i),\\ &y_{i,5}\equiv\mu(q_i),\ y_{i,6}\equiv\psi(q_i)\\ &\mathbf{y}_i\equiv\mathbf{y}(q_i)\equiv{}^T(y_{i,1},\ldots,y_{i,6})\equiv{}^T(\xi,\eta,\zeta,\lambda,\mu,\psi)\\ &\mathbf{Y}_j\equiv{}^T(y_{1,j},\ldots,y_{n,j}),\ j=1,6\\ &\mathbf{Y}\equiv(\mathbf{Y}_1,\ldots,\mathbf{Y}_6),\end{aligned}$$

where n is the *fixed* number of mesh points.

3.3.1. Choice of Q in CEPAM

The distribution function $Q(\mu,t)$ is set to be a linear combination of the integration variables:

$$Q(\mu,t)=\frac{\xi}{\Delta\xi}+\frac{\eta}{\Delta\eta}+\frac{\zeta}{\Delta\zeta}+\frac{\lambda}{\Delta\lambda}+\frac{\mu}{\Delta\mu} \tag{16}$$

The so-called distribution factors: $\Delta\xi$, $\Delta\eta$, $\Delta\zeta$, $\Delta\lambda$ and $\Delta\mu$ are free parameters. One finds that good results are obtained by setting these parameter to values close to the whole variation of each unknown:

$$\begin{aligned}&\Delta\xi=\xi(n)-\xi(1),\ \Delta\eta=\eta(n)-\eta(1),\ \Delta\zeta=\zeta(n)-\zeta(1),\\ &\Delta\lambda=\lambda(n)-\lambda(1),\ \Delta\mu=\mu(n)-\mu(1).\end{aligned} \tag{17}$$

These factors can be adjusted at each time step. Each unknown has therefore approximately a similar weight in the distribution function.

Note that the function $\theta(\mu,t)$ can now be explicitly calculated using Eqs. (7), (12), and (16).

3.3.2. Setting a grid point at a given location

At the transition between molecular and metallic hydrogen and, in a more general way, at any particular level where the density is discontinuous, the derivatives of the pressure, temperature and radius in respect to the mass are discontinuous functions. Between two mesh points, the piecewise polynomials which interpolate the unknowns are differentiable functions. Therefore their derivatives are allowed to be discontinuous only at a grid point. As a consequence, each discontinuity must be located precisely on a

knot. This allows one, with an *ad hoc* choice of the piecewise polynomial basis, to have different values on left and right for the derivatives of the function considered. For this delicate problem the use of the de Boor basis (see next section) is an elegant solution.

In order to simplify the discussion we will assume that there is only one level where a discontinuity arises (labeled with a subscript 'D'); naturally, in CEPAM, the algorithm is extended to several discontinuities, as long as the jumps of the density are separated by a sufficient number of grid points.

The localization of each discontinuity on a grid point is obtained by a slight modification of the algorithm used for the automatic allocation of grid points. The algorithm, developed by one of us (PM), is described hereafter; basically, it is an inverse linear interpolation.

The idea is the following: the grid points are located in such a way that from a mesh to the next the change of the distribution function is constant. Inside each mesh, indexed by i, the relative weights of the variables are defined by the distribution factors $\Delta\xi$, $\Delta\eta$, $\Delta\zeta$, $\Delta\lambda$, $\Delta\mu$. These are defined to within a factor $\omega_i(q)$, $i = 1, 2, \ldots, n-1$, which was implicitly assumed to be equal to one for each mesh. This factor can be adjusted (iteratively) in order to set each discontinuity limit on the closest grid point. In order to do so, instead of $Q(q)$, for $q \in [q_i, q_{i+1}[$, we use a weighted distribution function defined by pieces:

$$Q_i(q) \equiv Q(q)/\omega_i(q), \tag{18}$$

where $Q(q)$ is defined by Eq. (16). Analogously we set:

$$\psi_i(q) \equiv \frac{\partial Q(q)}{\partial q}/\omega_i(q),\ \theta_i(q) \equiv \frac{\partial Q(q(\mu))}{\partial \mu}/\omega_i(q), \tag{19}$$

the pieces of the function ψ_i being connected by continuity: $\psi_i(q_i) = \psi_{i-1}(q_i)$, $i = 2, \ldots, n-1$. Therefore, instead of Eq. (13), one uses:

$$\left(\frac{\partial \mu}{\partial q}\right)_t = \frac{\psi_i}{\theta_i}, \qquad \left(\frac{\partial \psi_i}{\partial q}\right)_t = 0. \tag{20}$$

We emphasize that $Q(q)$ and $\psi_i(q)$ are continuous but that $\omega_i(q)$ and then $\theta_i(q)$ are step functions. Due to the fact that i) the differential equations are not written at the mesh points, and ii) the spline/collocation method allows discontinuous derivatives at the mesh points, the discontinuities in Eq. (20) are handled in an implicit way (see Sect. 3.4).

Let us assume that, for the time t, a solution $\mathbf{Y}^{(0)}$ of the problem (14) has been initialized and that the weighted distribution function, defined by Eq. (18) with $\omega_i^{(0)}(q) \equiv 1$, is $Q_i^{(0)}(q)$. Each quantity with a '(j)' superscript will be related to the j-th iterated model, $j = 0, 1, \ldots$

At the location $q_{\rm D}^{(j)}$, where the discontinuity of density occurs, the distribution function, calculated with Eq. (16), amounts to $Q_{\rm D}^{(j)}$. Let l be the index of the nearest mesh point from the discontinuity ($l \neq 1, n$). Since $Q^{(j)}(q)$ is a strictly monotonous function, there is only a unique value $q_{\rm D}^{(j)}$ such that $Q^{(j)}(q_{\rm D}^{(j)}) = Q_{\rm D}^{(j)}$. Therefore, for $q \in [q_i, q_{i+1}[$, $i = 1, 2, \ldots, n-1$, the weights $\omega_i^{(j)}(q)$ can be defined for $j \geq 1$ by:

$$\omega_i^{(j)}(q) = \begin{cases} \dfrac{(Q^{(j-1)}(q_{\rm D}) - Q^{(j-1)}(q_{l-1}))}{\psi_i^{(j-1)}}, & \text{if } i = l-1, \\ \dfrac{(Q^{(j-1)}(q_{l+1}) - Q^{(j-1)}(q_{\rm D}))}{\psi_i^{(j-1)}}, & \text{if } i = l, \\ 1, & \text{otherwise.} \end{cases} \tag{21}$$

After convergence, Eq. (20) yields $\psi_i^{(\infty)}(q) = \text{Cte}$. From Eqs. (19) and (20) it follows that:

$$\psi_{l-1}^{(\infty)} = \frac{1}{\omega_{l-1}} \left\{ Q^{(\infty)}(q_l) - Q^{(\infty)}(q_{l-1}) \right\}.$$

On the other hand, Eq. (21) yields

$$\psi_{l-1}^{(\infty)} = \frac{1}{\omega_{l-1}} \left\{ Q^{(\infty)}(q_{\rm D}) - Q^{(\infty)}(q_{l-1}) \right\}.$$

Hence, one gets necessarily:

$$q_l = q_{\rm D}.$$

However, this first order iterative process will converge only if the functions considered are sufficiently smooth and if the discontinuity is sufficiently well defined. This is the case for the PPT. In CEPAM, the weights $\omega_i^{(j)}(q)$ are reevaluated after each Newton-Raphson correction. $Q^{(j)}(q)$ and $q_D^{(j)}$ are derived from the localization of the PPT at the $(j-1)$-th iteration.

Figure 2 illustrates the behavior of the solution when a mesh is adjusted on a discontinuity. First, only the mesh which is nearest to the discontinuity is significantly affected. Second, the first derivatives of the pressure and temperature are then clearly discontinuous, as required by the jump of the density (in the case of a homogeneous chemical composition this jump is about 20%). Finally, the solution is affected by about 10^{-3} if this algorithm is not used i.e. the PPT is not exactly localized on a grid point.

3.4. *Outlines of the spline/collocation method*

Since B-splines are not familiar in star or planetary interior modelings, we will briefly describe the principles of the spline/collocation method used for the integration of the two point boundary value problem. Refer to de Boor (1978) and Schumaker (1981) and to the literature cited herein for more advanced description and proofs.

With this technique all the unknown functions (e.g. pressure, temperature ..) are interpolated by piecewise

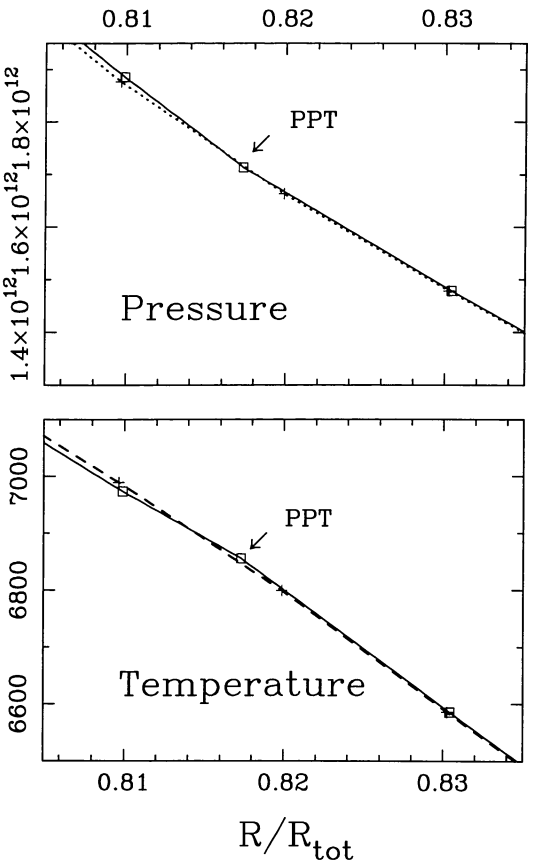

Fig. 2. Pressure (in dyn.cm^{-2}) and temperature (in K) profiles in a model for which a mesh point has been set at the location of the PPT (plain lines) and in a model for which the location of the meshes are free (dashed lines). The squares (resp. crosses) indicate the position of the mesh points corresponding to the plain lines (resp. dashed lines)

polynomials. One then writes that the differential equations of the planetary structure are fulfilled by these interpolating functions. If, for algebra, the canonical basis is the simplest way for writing piecewise polynomials, for the calculations, that basis leads to algorithms having bad stability conditions. Among all the basis of the linear set of piecewise polynomials, a local basis, the B-spline basis, leads to stable algorithms.

A B-spline is itself, obviously, a piecewise polynomial. It can be defined either from divided differences (de Boor 1978; Gaches 1988), or from the algorithm used for their calculation; in fact they are convolution products of the sampling Π ("door") function (Marchouk & Agochkov 1985).

3.4.1. The nodal vector: the key of the computations with B-splines

Before presenting in the definition of the B-splines, we must define more precisely what a piecewise polynomial $\mathcal{P}(q)$ of order s is, on a given partition Δ of $[1,n]$, $\Delta \equiv \{1 = q_1 < q_2 < \ldots < q_{n-1} < q_n = n\}$: $\mathcal{P}(q)$ is defined as a function which coincides, on each sub-interval $[q_i, q_{i+1}]$, $1 \leq i < n$, with a polynomial of degree $s-1$. The existence and uniqueness of $\mathcal{P}(q)$ on Δ results from the knowledge, at each breakpoint, of the kind of connection which is required between the right and the left pieces of polynomials. For instance, the so-called "natural spline" is a piecewise polynomial $\mathcal{P}_N(q)$ of order 4 (degree 3), constructed in such a way that, at the inner breakpoints q_i, $1 < i < n$, the second derivative $\mathcal{P}''_N(q_i)$ is continuous.

Formally, the rules of connection can differ from one breakpoint to the next: at some of them, $\mathcal{P}(q_i)$ can be discontinuous, at some others the left and right pieces can be tied fulfilling the continuity of their first derivatives or only of $\mathcal{P}(q_i)$,...etc. For each q_i, the connection is characterized by the so-called multiplicity m_i obtained as follow: let $d_i < s$, $1 < i < n$ be the order of the oscularity of the connection between the left and right polynomial pieces at the breakpoint q_i; $d_i = 0$ means continuity of $\mathcal{P}(q_i)$, $d_i = 1$ means continuity of the first derivative, $d_i = 2$ of the second ones ...etc. and we set $d_i = -1$ for a discontinuity of the function itself. At $i = 1$ and $i = n$ (inner and outer boundaries) we fix the value of $\mathcal{P}(q_i)$. This is equivalent to assume that $\mathcal{P}$ is discontinuous at these points. Hence, one has $d_1 = d_n = -1$. The multiplicity of the point q_i is then defined as:

$$m_i \equiv s - (d_i + 1)$$

From the vector of multiplicities: $\mathcal{M} = {}^T(m_1, \ldots, m_n)$ one constructs the heart of the calculation with B-spline: the so-called "nodal vector": $\mathcal{N}(\Delta,\ \mathcal{M},\ s)$ associated to the piecewise polynomial. It is the vector which has for coordinates the q_i, each of them appearing m_i times. $\mathcal{N}$ can be written as:

$$\begin{aligned}\mathcal{N} &= {}^T(\overbrace{q_1, q_1, \ldots, q_1}^{m_1}, \overbrace{q_2, q_2, \ldots, q_2}^{m_2}, \ldots, \overbrace{q_n, q_n, \ldots, q_n}^{m_n}) \\ &\equiv {}^T(t_1, t_2, t_3, \ldots, t_{S+m_n}).\end{aligned}$$

The dimension of $\mathcal{N}$ is then $S + m_n$, with $S = \sum_{i=1}^{n-1} m_i$. A convenient schematic representation of the nodal vector consists in writing one column of m_i elements for each breakpoint q_i.

As an example, with $s = 4$, $n = 6$, continuity of $\mathcal{P}(q)$ at q_3, of $\mathcal{P}'(q)$ at q_6, of $\mathcal{P}''(q)$ at q_2 and q_5, and discontinuity of $\mathcal{P}(q)$ at q_4, the nodal vector is represented as:

×	×	×	×	×	×	×
×		×	×		×	×
×		×	×			×
×			×			×

Once given this nodal vector, the value of the k-th, $1 \leq k \leq S$, normalized B-spline on $\mathcal{N}$ is obtained by induction:

$$N_k^1(q) = \begin{cases} 1, & \text{if } t_k \leq q < t_{k+1}, \\ 0, & \text{otherwise,} \end{cases} \qquad (22)$$

and, for $1 < \sigma \leq s$:

$$N_k^\sigma(q) = \frac{q - t_k}{t_{k+\sigma-1} - t_k} N_k^{\sigma-1}(q) + \frac{t_{k+\sigma} - q}{t_{k+\sigma} - t_{k+1}} N_{k+1}^{\sigma-1}(q). \quad (23)$$

Note that its first derivative can easily be calculated:

$$\frac{dN_k^s(q)}{dq} = (s-1)\left[\frac{-N_{j+1}^{s-1}(q)}{t_{k+s} - t_{k+1}} + \frac{N_j^{s-1}(q)}{t_{k+s-1} - t_k}\right]. \quad (24)$$

From these relationships one can see that $N_k^s(q) \equiv 0$ if $q \notin [t_{k-s+1}, t_{k+s}]$. Hence the B-spline basis is a local basis. Moreover, $\forall q \in [1, n]$, only s B-splines of order s are not identically zero and their sum is equal to 1. We stress that formally, Eqs. (22) and (23) do not constitute a mathematically correct definition for the B-splines since some denominators in Eq. (23) vanish. However, when this happens, the corresponding B-spline is identically zero and this term has therefore no contribution. Since only s splines have to be calculated for a given point q, an algorithm which avoids zero denominator can easily be derived from Eqs. (22) and (23) (see de Boor 1978). Finally, it can be shown that the set $\mathcal{B}(\Delta, \mathcal{N}, s)$ of all the B-splines $N_k^s(q)$, $1 \leq k \leq S$, forms a basis for the linear space of the set of the piecewise polynomials having $\mathcal{N}$ for nodal vector. Thus, the dimension of $\mathcal{B}$ is precisely S.

3.4.2. Integrating differential equations with the spline/collocation method

Since the system of Eq. (14) is non linear, it is solved by iterations from an initial model of the planet (which can be calculated, for instance, by a shooting method or using a polytropic approximation). Let us suppose that we have such a model, representing fairly well the interior of a planet. Each of the functions $\mathbf{Y}_j^{(0)}(q), j = 1, \ldots, 6$ which describes this starting model is known for a discrete set of mass (or radius) values; it can be interpolated by a piecewise polynomial. Then, with respect to a B-spline basis, $\{N_k^s(q)\}_{k=1}^S$ of order s, at q, for the variable j, the piecewise polynomial is developed as:

$$\mathcal{P}_j(q) = \sum_{k=1}^{S} p_{k,j} N_k^s(q), \quad (25)$$

where the $p_{k,j}$ are the coordinates of the j-th unknown with respect to the B-spline basis. (These coordinates verify the linear systems obtained by writing that the interpolation functions coincide with the functions at each grid point.) The unknowns can be taken as the B-spline coefficients $p_{k,j}$, $1 \leq j \leq 6$, $1 \leq k \leq S$, rather than the functions themselves. Note that for a given q, only s coefficients are non identically zero: the sum in Eq. (25) has only s non zero terms. Formally, each of the differential equations in the system (14) , can be expressed for the $p_{k,j}$ in the form:

$$\frac{\partial \mathcal{P}_j(q)}{\partial q} = \sum_{k=1}^{S} p_{k,j} \frac{\partial N_k^s(q)}{\partial q}$$

Hence, derivatives of the functions can be readily calculated by derivation of the basis function $N_k^s(q)$.

In CEPAM the de Boor's B-spline basis is used. In the case of first order differential equations (which do not involve second derivatives of the unknown functions), the continuity of the piecewise polynomial is ensured at the knots but not their subsequent derivatives. Hence, the nodal vector has the schematic representation:

× × × ... × × ×
× × for s=2,

and

× × × ... × × ×
× × × ... × × ×
× × for s=3.

This allows one to obtain the B-spline functions shown in Fig. 3. It is clear that the continuity of the derivatives of the functions is not ensured at the mesh points (contrary to the common interpolation with natural cubic splines). This does not mean that the function derivatives will be discontinuous but rather that they *can* be discontinuous at these points. (This property has been used in the previous section in order to treat exactly the discontinuities.)

For each mesh and for each piecewise polynomial, s parameters have to be known (recall that $\mathcal{P}(q)$ is, on $[q_i, q_{i+1}]$, a polynomial of degree $s-1$). Since, for each unknown, the continuity of the function or the boundary conditions of the problem provide one constraint, the equations have to be written at $s-1$ points within each mesh. These are called the *collocation points*, noted $(\tau_k)_{k=1}^{S-1}$, where $S = (n-1)(s-1)+1$ and are defined as follow:

$$\begin{cases} -1 \leq \alpha_1 < \alpha_2 < \ldots < \alpha_{s-1} \leq 1, \\ \tau_{(i-1)s+\sigma} \equiv \frac{1}{2}\left[q_{i+1} + q_i + \alpha_\sigma (q_{i+1} - q_i)\right], \\ \qquad\qquad i = 1, \ldots, n;\ \sigma = 1, \ldots, s-1. \end{cases} \quad (26)$$

The quantities α_σ can be almost arbitrarily chosen. However, for the de Boor's nodal vector, they are chosen as the zeros of the $(s-1)$-th Legendre polynomial. (The same method is used in the standard Gauss quadrature; note that these points are then different from the mesh points q_i.) For this particular collocation pattern, it can be demonstrated that, for first order differential equations, the overall approximation is of order $O(1/n)^s$, but that it is of order up to $O(1/n)^{2(s-1)}$ at the mesh points (de Boor & Swartz 1973). This is the so-called "superconvergence".

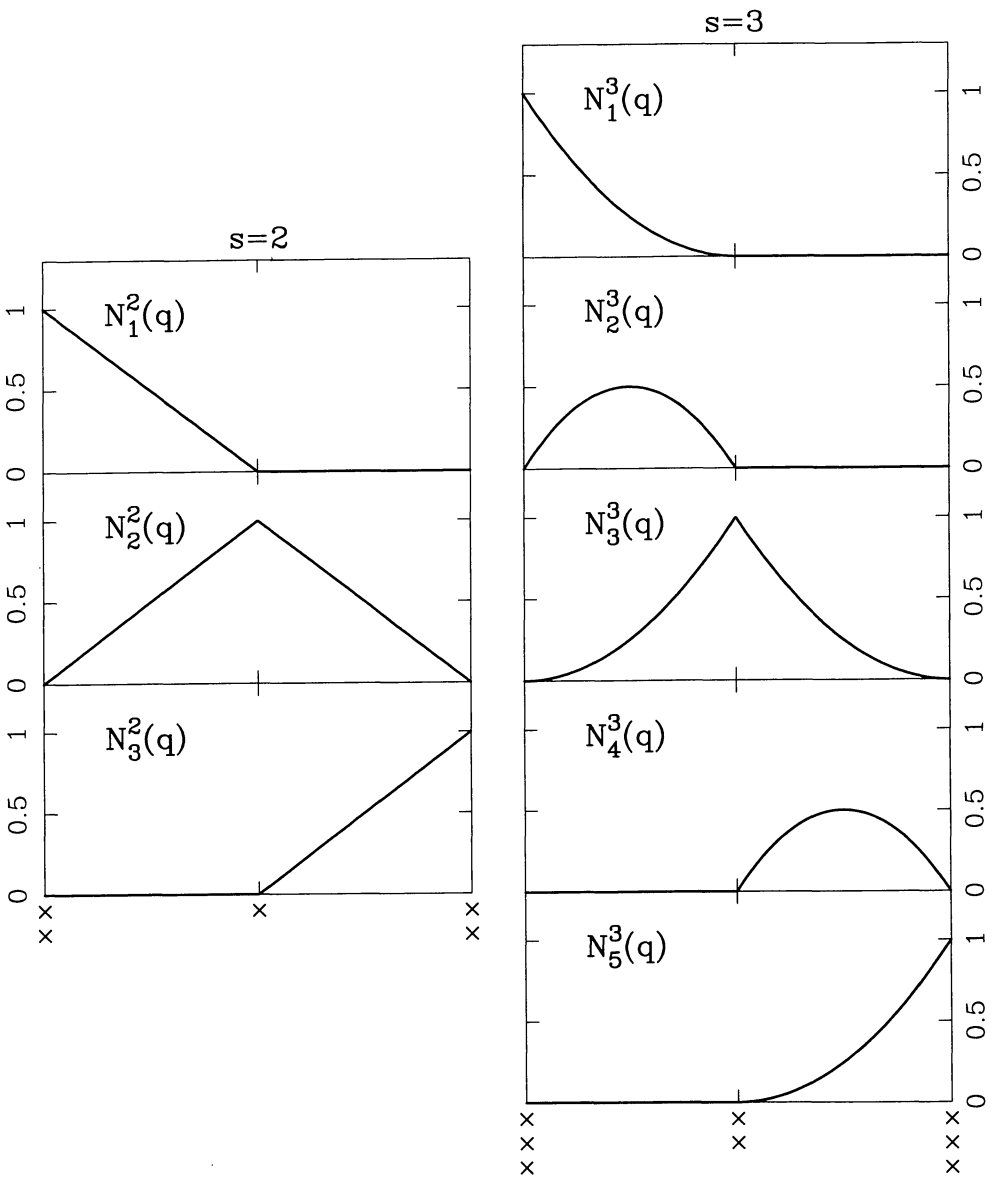

Fig. 3. Normalized B-splines of order s=2 (left) and s=3 (right) calculated with de Boor basis for n=3 equidistant mesh points. The nodal vectors are indicated by crosses below both graphs

Once written on this particular basis, system (14) (including boundary conditions at both ends) can be expressed in a simplified form as:

$$\mathcal{F}_j(q;\mathbf{P}) = 0, \qquad j = 1,\ldots,6. \tag{27}$$

where $\mathcal{F}_j$ is a function of q and of the vector $\mathbf{P}$ of the coordinates $p_{k,j}$, $k = 1,\ldots,S$, $j = 1,\ldots 6$. The resolution of the non linear system of equations Eq. (27) is obtained by linearization (Newton-Raphson method) starting from the initial model. Since the B-splines basis is a *local* basis, the jacobian matrix is block-diagonal. This allows storage facilities and faster calculations. In CEPAM one usually uses either $s = 2$ or $s = 3$ for the order of the piecewise polynomials. The linear system to be solved has then one of the following structures:

with $s = 2$:

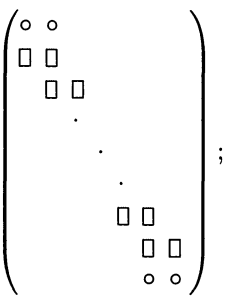

with $s = 3$:

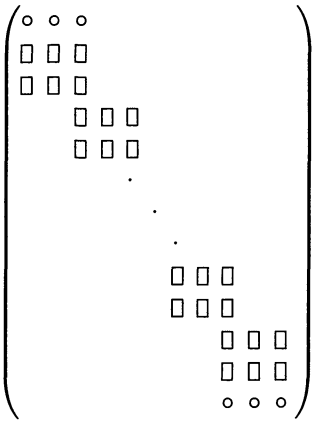

The "□" are 6×6 matrix for the collocation points and the ∘ are 3×6 matrix for the boundaries. The resolution of the linear system of equations is performed using partial gaussian pivoting. The robustness of the solution is improved by using the modified Newton-Raphson method (see e.g. Stoer & Bulirsch 1980), giving the values of the unknown functions at iteration $l+1$ from their values at iteration l:

$$p_{k,j}^{(l+1)} = p_{k,j}^{(l)} - \alpha\, dp_{k,j}^{(l)} \qquad k = 1, \ldots, S;\ j = 1, \ldots, 6. \tag{28}$$

where $dp_{k,j}^{l}$ are the corrections and α is a parameter which ensures that variations of the unknowns $p_{k,j}$ remain small even when $dp_{k,j}^{l}$ is large (hence, $\alpha \leq 1$). The iteration stops when a sufficient accuracy is reached.

A disadvantage of the use of the linearization technique is the need of first and second derivatives of the density and internal energy (or entropy) obtained from the EOS with respect to pressure and temperature. Hence, one has to rely on the accuracy and consistency of the EOS, which can sometimes be problematic. Note however that this can affect the convergence of the solution but not its accuracy.

3.5. *Optimization of static models*

Like the Sun which is calibrated to the observed radius and luminosity by using free parameters, models of the giant planets are adjusted to observed quantities by using parameters which are not fixed by observations or physical arguments. This is for instance the case of the mass and structure of the central dense cores of these planets.

The observational quantities which are directly related to the structure of the interior of the planets are the equatorial radius $R_{\rm eq}$ and the gravitational moments J_2, J_4 and J_6 (see e.g. Lindal 1992). These are called *primary constraints* of the models to distinguish them from *indirect* constraints on the internal structure, as the chemical composition of the atmosphere. We will therefore seek to obtain optimized models, i.e. models which reproduce the primary constraints within their error bars.

Let us call x, y and z three free parameters of the problem: the core mass, the chemical composition of the interior, and a jump of composition at the transition between molecular and metallic hydrogen (PPT). (Evidently, many more free parameters could possibly be imagined but a wiser philosophy is to follow the principle of Ockham's razor and thus to limit the number of these parameters.) We introduce the following minimization function:

$$f(x,y,z) = \frac{1}{4}\left[\left(\frac{R_{\rm eq}^{\rm calc} - R_{\rm eq}^{\rm obs}}{\sigma^{\rm obs}(R_{\rm eq})}\right)^2 + \left(\frac{J_2^{\rm calc} - J_2^{\rm obs}}{\sigma^{\rm obs}(J_2)}\right)^2 + \right.$$
$$\left. + \left(\frac{J_4^{\rm calc} - J_4^{\rm obs}}{\sigma^{\rm obs}(J_4)}\right)^2 + \left(\frac{J_6^{\rm calc} - J_6^{\rm obs}}{\sigma^{\rm obs}(J_6)}\right)^2\right], \tag{29}$$

where $\sigma^{\rm obs}(X)$ is the $1\,\sigma$ error bar on the observed quantity X. The index 'calc' refers to quantities calculated by the code. Optimized models are such that $f < 1$: all the primary constraints are then satisfied to $2\,\sigma$. An even better optimization is performed when reaching smaller values of f.

One could think of using a gradient method (or any related algorithm) to find the minimum of f. However, since we seek an accuracy which is better than 10^{-4} on $R_{\rm eq}$ and J_2 the optimization problem is highly unstable. On the other hand, the calculation of a jacobian not only requires calculation of 3×3 models at each time, but can also be achieved only with numerical derivatives whose accuracy can sometimes be quite weak. Therefore, the minimization of f is best achieved using a simplex method (see Press et al. 1986) which is a generalization of bisection at more than 1 dimension. The algorithm used is such that the volume of the simplex (a tetrahedron in our case) could not increase from one iteration to the next. This ensures that two consecutive models are not too far from each other and therefore yields much better convergence to the solution and higher accuracy.

As a result a minimization successfully matching the primary constraints requires an accuracy of about 10^{-6} on the value of the free parameters. This precision is unrealistic compared to the uncertainties of the physics involved (EOS, opacities, rotation...etc.). However our goal is *not* to obtain this precision but rather to determine whether it is possible to find $f < 1$, and then to estimate the extent of the set of solutions. This can be achieved using the method presented here.

4. Accuracy

A first test of the code and its accuracy is to compare solutions obtained from CEPAM with analytic solutions. The comparison with a polytrope of index $n = 1$ (see e.g. Chandrasekhar 1939) is presented in Fig. 4. This is obviously a crude simplification over the real structures of the giant planets. In particular the models have been calculated with a perfect gas EOS and no core. Notwithstanding, this allows an estimation of the accuracy of the

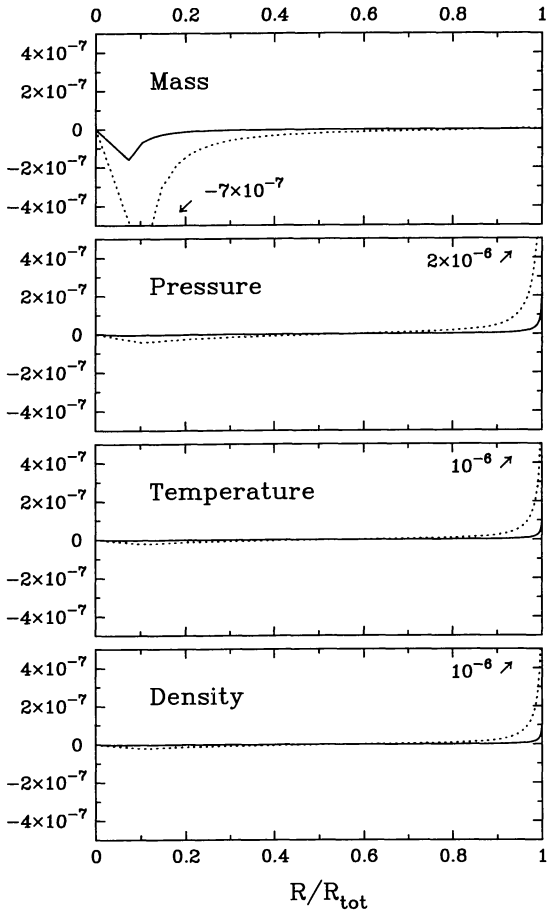

Fig. 4. Accuracy of solutions obtained with CEPAM calculated by comparison with a polytrope of index $n = 1$. The dashed lines represent models with 100 meshes whereas plain lines indicate models with 200 meshes. The order of the piecewise polynomials used in the collocation method is $s = 3$ for both models

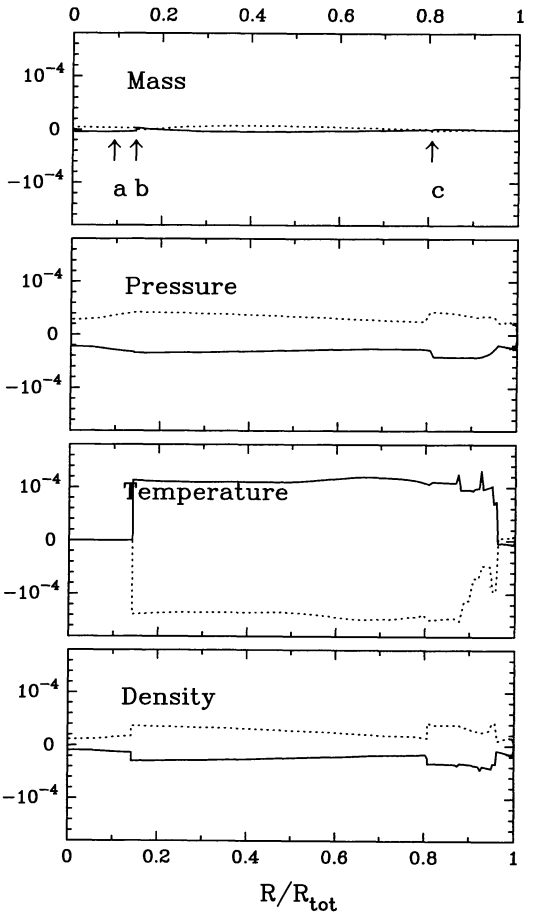

Fig. 5. Accuracy of Jupiter models obtained with 100 (dotted lines) and 200 mesh points (plain lines). These models are compared to a 500 mesh points model. As previously, the order of the piecewise polynomials used is always $s = 3$. The letters a, b, and c indicate the levels where a discontinuity occurs: a) Rock/Ice transition in the core. b) Rocky core/H–He envelope. c) Metallic/Molecular hydrogen (PPT). Note that the zero error on the temperature of the core is simply a consequence of our isothermal assumption

solutions. As a result, an extremely precise solution (about 10^{-8} or 10^{-9} for 100 and 200 mesh points, respectively) is found in the largest part of the planet. The accuracy is somewhat lower at the center and near the surface. This stems from the fact that the mass shrinks rapidly near the center, as well as the other quantities near the surface. Thus, one cannot avoid lesser precision in these regions. However, we stress that with a relatively low number of points (100) the accuracy of the solution is better than $2\ 10^{-6}$ everywhere. This latter quantity shrinks by more than one order of magnitude when the number of points is doubled, in agreement with the fact that the order of the scheme is, at the mesh points, $2(s-1) = 4$ when using third order piecewise polynomials.

An internal test of models of Jupiter is presented in Fig. 5. We see that the accuracy of a "real" interior model is much worse than that obtained by comparison with an ideal model (the polytrope). This stems from the fact that the structure of a polytrope is an oversimplification of the problem. As a result, the mass is still obtained with a good precision (about 10^{-6}) but this is not the case for the other quantities. In particular, systematic errors are found both for models with 100 and 200 mesh points. These errors do not shrink significantly when doubling the number of meshes (and hence one could have doubts about the precision of the model with 500 meshes), but rather seem to be random functions of the total number of points in the model.

The cause of these errors is readily understood when looking at Fig. 6. The adiabatic gradient is a quantity which comes directly from the equation of state. Furthermore, it is calculated as:

$$\nabla_{ad} \equiv -\frac{(\partial S/\partial \ln T)_P}{(\partial S/\partial \ln P)_T},$$

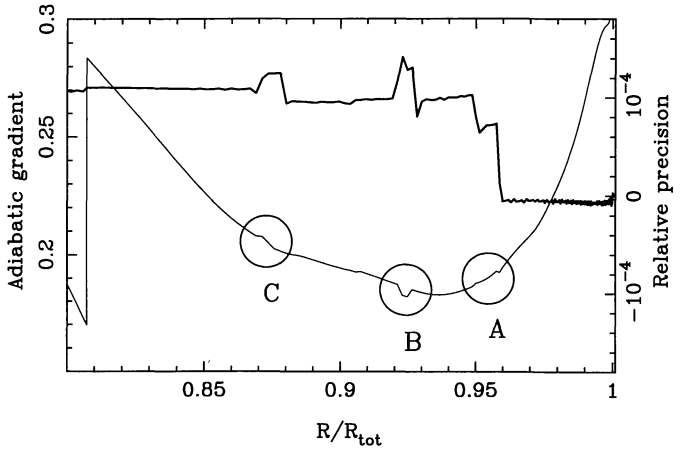

Fig. 6. Comparison of the adiabatic gradient (thin line) to the accuracy of the temperature (strong line) obtained using data from Fig. 5. The letters A, B and C indicates levels where misbehaviors of the equation of state occur (see text)

where S is the specific entropy of the mixture of hydrogen and helium, calculated with an ideal-volume law approximation involving the specific entropies of pure hydrogen and of pure helium (see Chabrier et al. 1992; Guillot et al. 1994b). Hence, this calculation involves four first derivatives, which are calculated using cubic-splines interpolations. It is therefore not very surprising that such kinks occur in a region which is close to a border of the EOS table, and difficult to modelize, due to the dissociation of the hydrogen molecule. This yields inaccuracies of about 0.1% to 5% on the adiabatic gradient. Depending on their extent, these kinks will eventually be avoided by models with a relatively low number of meshes but will be seen when the number of meshes is increased. This is indeed the case in the region labeled "A" in Fig. 6: models with 100 and 200 mesh points do not experience this misbehavior of the adiabatic gradient whereas it is treated by the model with 500 mesh points. The extent of kinks "B" and "C" is somewhat more important and they have therefore less influence on the accuracy of the temperature profile. Furthermore, the functions to be integrated are then not "sufficiently smooth" and convergence theorems do not apply any more for this level of accuracy. Therefore, the precision of the models is limited to about 10^{-4} due to the equation of state and not to the algorithm presented here. One could argue that the discontinuities seen on the adiabatic gradients are due to an inaccuracy of the temperature profile rather than the opposite. This is not the case: first because in the region considered ($P < 1$ Mbar), pressure ionization and dissociation of hydrogen cannot produce relative variations of the adiabatic gradient of more than 1% when P or T are changed by only 10^{-4}, and second because this phenomenon occurs independently of any modeling.

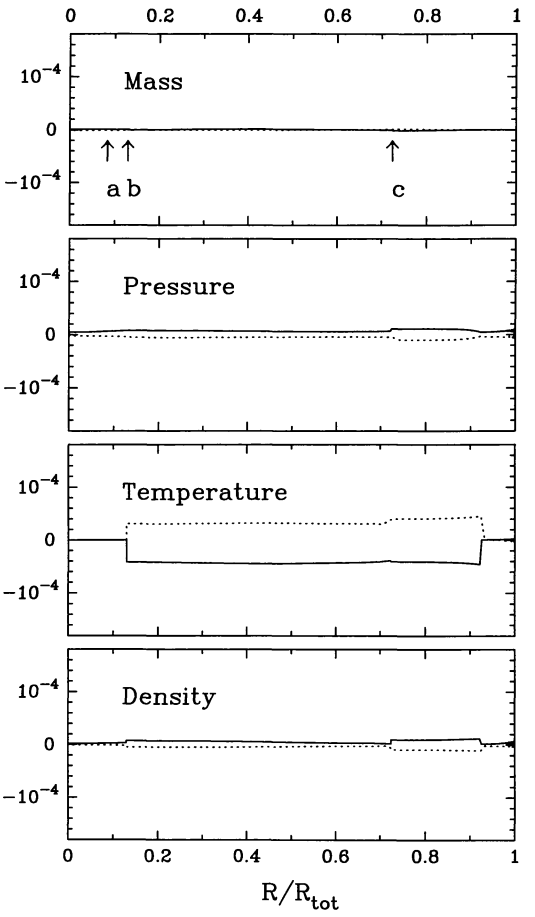

Fig. 7. Same as Fig. 5 for a pure hydrogen EOS

These problems are reduced when considering the EOS for pure hydrogen. Even though we cannot calculate a physically consistent model of Jupiter with such an EOS, it is nevertheless possible to estimate the accuracy of the solution calculated by CEPAM code. This is done in Fig. 7. The accuracy of the solution is then considerably increased, but is still limited by a faint jump of the adiabatic gradient ($\sim 1\%$) for $P \approx 0.16$ Mbar. As a result all variables have a precision which is better than $2\ 10^{-5}$ except the temperature for which this value is double, with models with only 100 or 200 mesh points. Furthermore, the discontinuities which were predictable (labeled a, b and c in Figs. 5 and 7) have been treated with an accuracy which is better than 10^{-5}.

We present the results obtained for the quantities related to the rotation of the planet, i.e. equatorial radius and gravitational moments, for a "real" model of Jupiter (corresponding to Fig. 5) in Fig. 8. These results are consistent with the precisions obtained in Fig. 5: the equatorial radius is calculated with an accuracy which is better than 10^{-4} for models calculated with 100 mesh points or more and of order $s = 3$. The calculation of the other quantities, J_2 and J_4, involves powers of the equatorial

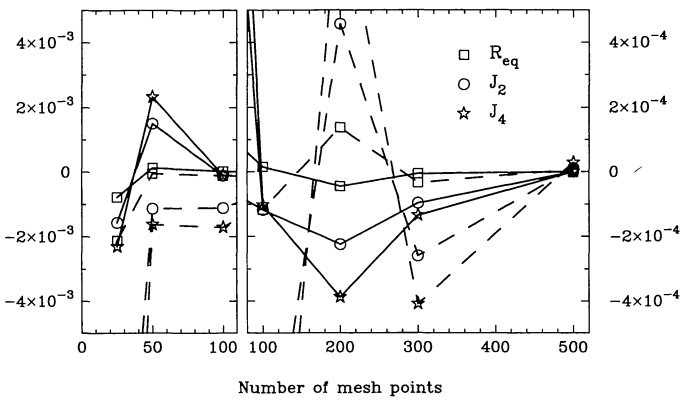

Fig. 8. Relative variations of the equatorial radius R_{eq} (squares) and gravitational moments J_2 (circles) and J_4 (stars) as a function of the number of mesh points used in CEPAM models. Points connected by plain lines indicate calculations with third order piecewise polynomials ($s = 3$). Points connected by dashed lines indicate calculations with second order piecewise polynomials ($s = 2$). Note that the scale of the Y–axis is different on left and right graphs. All results are compared to $s = 3$ models with 500 mesh points

radius and their precisions are lowered accordingly. It is interesting to see that, as expected, the accuracy of models with order of piecewise polynomials set to $s = 2$ is worse than when $s = 3$ and that both models have a better precision when the number of meshes increases (this is not always true since the variations are essentially random, but reflects the global tendency). Thus models with 500 mesh points calculated with $s = 2$ and $s = 3$ are very similar. Furthermore, the convergence is consistent with theoretical previsions only for low numbers of mesh points (25 or 50). This stems from the effect discussed previously: the misbehaviors of the EOS are not seen by models with a low number of meshes. Hence, the functions can then be considered as sufficiently smooth. This is not any more the case when more precise models are calculated. Finally, the presence of discontinuities (as the PPT) limits the order of convergence, but this is a small effect.

These results can be compared to the precision obtained from the observations: for Jupiter (for which we have the most accurate data) R_{eq}, J_2 and J_4 are known to about $6\ 10^{-5}$, $7\ 10^{-5}$ and $9\ 10^{-3}$. Thus, the accuracy of R_{eq} and J_2 given by models with 100 or 200 mesh points is comparable to the accuracy of the observations. This is problematic, mainly for the optimization procedure. Hence, the use of a very robust algorithm, as described in Sect. 3.5 is highly valuable.

An important point is then the accuracy of the solutions calculated within the theory of figures. Due to the unpleasant aspect of the equations, the development of the theory was limited to the third order, as it is usually the case. For this order of approximation, the accuracy of the solutions for J_2 is well below the observational constraints (see Appendix).

However, as pointed out by Hubbard (1982), the differential rotation in Jupiter and Saturn yields an uncertainty on the value of J_2 which is one order of magnitude larger than the observational error bar (see Lindal 1992), and is therefore compatible with a third order calculation. On the other hand, the theoretical uncertainties on J_4 and J_6 are compatible with the observations. Hence, without a real understanding of the rotation of the interior of these planets, only a slight improvement in the gravitational constraints can be expected by carrying the theory of figures to a higher order.

5. Conclusion

In this paper, we have described the numerical techniques used in CEPAM, a flexible, robust and precise tool designed for the computation of the internal structure of the giant planets.

The interior including a rocky core (possibly surrounded by a mantle of ices), is calculated without the assumption of full adiabaticity. From our knowledge it is the first numerical code which allows such a complete computation.

This code has been used for the construction of non-adiabatic models (i.e. with a radiative zone) of Jupiter and Saturn. Furthermore, it enables a precise determination of the free parameters of the models. This allows one to study the non-uniqueness of the solutions, which is particularly significant in the case of Saturn (Guillot et al. 1994b).

The method employed consists of an interpolation by piecewise polynomials of the unknown functions which describe the internal structure. The resolution of the quasi-static equilibrium, a two point boundary value problem, employed a spline/collocation technique originated by de Boor (1978). Among the most interesting advantages of the method, we point out its stability and the fact that the discontinuities of the unknown functions, or of their derivatives, are more easily worked out than with finite differences. Another convenient feature, is that the order of accuracy is monitored by only one external parameter.

Furthermore, a robust algorithm, derived from the simplex method, has been worked out for the optimization of the models. It allows one to infer the values of the three most important free parameters of the model (e.g. the mass of the core, the chemical composition and the jump of composition at the PPT) from the observed values of the equatorial radius and the gravitational moments J_2, J_4 and J_6.

The comparisons of models computed with different number of shells and with different order of accuracy allowed us to estimate the internal relative accuracy of our models. So far, it is limited by the precision of the interpolation scheme of the tabulated equation of state at the

level 10^{-4}. This value decreases to a few 10^{-7} if a perfect gas equation of state is employed.

It appears that the internal relative accuracy of the models with only 100 mesh points and parabolic splines is limited not by numerical considerations but by some faint inconsistencies of the equation of state. We conclude that the models of giant planets computed with CEPAM have the accuracy of the input physics.

On a separate matter, the problem of the evolution of a non-adiabatic planet is an extension of the numerical methods described here and will be treated in a forthcoming paper.

Acknowledgements. We wish to thank Oluş Boratav and Bill Hubbard for helpful comments on the manuscript.

Appendix: theory of figures

We outline in this appendix the treatment of the rotation used in modeling giant planets. The theory dealt with is long-known from planetary workers and was introduced by Clairaut and Laplace who calculated first order solutions. A second order theory is due to Darwin and De Sitter and was applied to Jupiter and Saturn by DeMarcus (1958). Interior models, including ours generally use a 3rd order theory, although Zharkov & Gudkova (1992) solve the equations of the theory of figures to 5th order. A detailed review is found in Zharkov & Trubitsyn (1978), including the equations to 3rd order which will not be given here. Moreover we will assume that the rotation is solid (for a discussion of the effect of differential rotation on the interiors of Jupiter and Saturn, see Hubbard 1982).

In order to estimate the influence of rotation on the structure of the giant planets, we introduce a small parameter m which is the ratio of the centrifugal to gravitational acceleration:

$$m = \frac{\omega^2 R_{\rm tot}^3}{G M_{\rm tot}}, \qquad (1)$$

where R is the mean radius of the planet. m is approximately equal to 0.08, 0.14, 0.04 and 0.02 for Jupiter, Saturn, Uranus and Neptune, respectively.

The basic problem of the theory of figures is the determination of level surfaces on which the gravitational potential remains constant. In the case of hydrostatic equilibrium the other quantities density, pressure ...etc, are also constant on these level surfaces.

In order to determine these surfaces, the radius is sought in the form:

$$r(\beta,\theta) = R_{\rm tot}\beta\left\{1+\sum_{i=0}^{\infty} s_{2i}(\beta)P_{2i}(\cos\theta)\right\}, \qquad (2)$$

where θ is the polar angle, β is the normalized mean radius, P_i are Legendre polynomials and s_i are functions to be calculated and of order of smallness m^i (except s_0 which is of order of smallness m^2). Furthermore, it can be shown that the total potential (gravitational+centrifugal) can also be developed as a sum of spherical harmonics:

$$U(r,\theta) = \frac{4}{3}\pi G\bar{\rho}R_{\rm tot}^2\,\beta^2\sum_{i=0}^{\infty} A_{2i}(\beta)P_{2i}(\cos\theta), \qquad (3)$$

where $\bar{\rho}$ is the mean density and $A_{2i}(\beta)$ are non-dimensional quantities. Requiring that U be constant on level surfaces one obtains $A_{2i}=0$ for $i>0$.

A theory of order n can then be calculated by truncation of Eqs. (2) and (3) for $i>n$. In other words, we suppose that $s_{2i}(\beta)\equiv 0$ when $i>n$. The remaining non-zero s_{2i} parameters are solution of an implicit set of integro-differential equations determined by the n conditions on A_{2i}:

$$\begin{cases} s_{2i} = f_{2i}(\beta, s_0, s_2, \ldots, s_{2n-2}), & \text{for } i<n,\\ s_{2n} = f_{2n}(\beta, s_0, s_2, \ldots, s_{2n-2}, s_{2n}), \end{cases} \qquad (4)$$

and f_{2i} are non-linear functions of the variables $\beta, s_0, \ldots, s_{2n}$. The calculation of these functions requires integrals of the form

$$S = \int \rho(\beta)\,{\rm d}f(\beta, s_0, \ldots, s_{2n}),$$

which are calculated as:

$$S = \sum f(s_i, s_{0i}, \ldots, s_{2n\,i})\Delta\rho_i - \int f(\beta, s_0, \ldots, s_{2n})\frac{{\rm d}\rho}{{\rm d}\beta}{\rm d}\beta.$$

$\Delta\rho_i$ are the discontinuities of the density at point s_i, including the two boundaries. This method allows one to take more easily into account the discontinuities of the density. Moreover, the accuracy of the derivative ${\rm d}\rho/{\rm d}\beta$ can be checked directly from the interior model. This quantity has been calculated using directly the equations for the quasi-static equilibrium and the derivatives of the EOS.

System (4) was solved with an explicit method. The order of convergence is only 1 but this is sufficient since this system is rapidly convergent (about 20 iterations are needed at the first time that these equations are solved).

The total gravitational potential is then determined using Eq. (3) and reported in the equation of hydrostatic equilibrium:

$$\nabla P = \rho\nabla U. \qquad (5)$$

A convenient method is to develop $A_0(\beta)$ as:

$$A_0(\beta) = B_0(\beta) + \frac{M}{M_{\rm tot}\beta^3} + \frac{1}{\beta^2}\int_\beta^1 \frac{\rho(\beta')}{\bar{\rho}}\frac{d}{d\beta'}\left[\beta'^2\left(\frac{3}{2}+h(\beta')\right)\right]{\rm d}\beta' - \frac{1}{3}m,$$

where $B_0(\beta)$ and $h(\beta)$ are slowly varying functions of β and are of order of smallness m^2. It can then be easily shown by using Eqs. (1), (3), and (5) that:

$$\frac{dP}{dM} = -\frac{GM}{4\pi R^4} + \frac{\omega^2}{6\pi R} + \frac{GM_{\rm tot}}{4\pi R_{\rm tot}^3 R}\varphi_\omega, \qquad (6)$$

φ_ω being defined by:

$$\varphi_\omega = 2\left[B_0(\beta) - \frac{\rho(\beta)}{\overline{\rho}}h(\beta)\right] + \beta\left[B_0'(\beta) - \frac{\rho(\beta)}{\overline{\rho}}h'(\beta)\right] \quad (7)$$

The functions B_0 and h are then interpolated as a function of β using cubic piecewise polynomials with a nodal basis ensuring discontinuous behaviors where (physical) discontinuities occurs. As a result, the centrifugal potential is at most equal to 6% and 10% of the total gravitational potential for Jupiter, and Saturn respectively. The term φ_ω increases slowly from about 2 10^{-3} at the center to 4 10^{-3} at the 1-bar level of Jupiter, and to 10^{-2} at the 1-bar level of Saturn.

The external gravitational potential $V_{\rm ext}$ can also be expressed in the form of a development of Legendre polynomials:

$$V_{\rm ext}(r,\theta) = \frac{GM}{r}\left\{1 - \sum_{i=1}^{\infty}\left(\frac{R_{\rm eq}}{r}\right)^{2i} J_{2i}P_{2i}(\cos\theta)\right\}, \quad (8)$$

where $R_{\rm eq}$ is the equatorial radius of the planet. The coefficients J_{2i} are the gravitational moments, which are, for the giant planets, of order m^i. These coefficients can be determined for a given interior model, using Eq. (4). Furthermore, J_2, J_4 and J_6 have been directly measured in the four giant planets and thus provide fundamental constraints for interior models (see Sect. 3.5).

The algorithm has been tested with the analytic polytropic solutions to order 4 calculated by Hubbard et al. (1975). This comparison reveals that the precision of a third order algorithm is superior to the observational accuracy on J_6 but is of the same order for J_4 and insufficient for J_2 for Jupiter and Saturn (see Lindal 1992). This stems from the fact that the relative accuracy on the measured value of J_2 for Jupiter is 7 10^{-5} whereas our calculations have an accuracy of $\sim$ 3 10^{-3}. In fact, since we calculate J_2 to the order of smallness m^3 and since $J_2 \propto m$ we cannot expect a much larger accuracy than $m^2 \approx 6\ 10^{-3}$ (for Jupiter). This problem is discussed in Sect. 4.

References

Bézard B., Baluteau J-P, Marten A. 1983, Icarus 54, 434

Chabrier G., Saumon D., Hubbard W.B., Lunine J.I. 1992, ApJ 391, 817

Chandrasekhar S. 1939, Stellar Structure (Dover Publications Inc., New-York) second ed. 1957

de Boor C. 1978, A Practical Guide to Splines (Springer–Verlag New York, Heidelberg, Berlin) third ed. 1985

de Boor C., Swartz B. 1973, SIAM J. Numer. Anal. 10, 582

DeMarcus W.C. 1958, AJ 63, 2

Eggleton P.P. 1971, MNRAS 151, 351

Gaches J. 1988, Modélisation de Courbes et surfaces Splines, Ecole Nationale Supérieure d'Ingénieurs de Constructions Aéronautiques, Toulouse

Graboske H.C., Pollack J.B., Grossman A.S., Olness R.J. 1975, ApJ 199, 265

Guillot T., Gautier D., Chabrier G., Mosser B. 1994a, Are the giant planets fully convective? Icarus 112, in press

Guillot T., Chabrier G., Morel P., Gautier D. 1994b, Non-adiabatic models of Jupiter and Saturn, Icarus 112, in press

Henyey L.G., Le Levier R., Levee R.D. 1959, ApJ 129, 2

Hubbard W.B. 1982, Icarus 52, 509

Hubbard W.B., Marley M.S. 1989, Icarus 78, 102

Hubbard W.B., Slattery W.L., DeVito C.L. 1975, ApJ 199, 504

Jeffreys H. 1923, MNRAS 83, 350

Kippenhahn R., Weigert A. 1991, Stellar Structure and Evolution (Springer Verlag, Berlin)

Lindal G.F., Wood G.E., Levy G.S. et al. 1981 J. Geophys. Res. 86, 8721

Lindal G.F. 1992, AJ 103, 967

Marchouk G., Agochkov V. 1985, Méthode des Eléments Finis, Mir

Morel P. 1989, In Cours de Structure Interne, eds. A.M. Hubert & E. Schatzman, Publ. Observatoire de Paris, Section Meudon, 117–123

Mosser B., Gudkova T., Guillot T. 1994. The influence of the troposphere on giant planets oscillations, A&A, in press

Press W.H. Flannery B.P. Teukolsky S.A. Vetterling W.T. 1986, Numerical Recipes (Cambridge University Press, Cambridge)

Saumon D., Chabrier G. 1991, Phys. Rev. A 44, 5122

Saumon D., Chabrier G. 1992, Phys. Rev. A 46, 2084

Saumon D., Hubbard W.B., Chabrier G., Van Horn H.M. 1992, ApJ 391, 827

Schumaker L.L. 1981, Spline Functions: Basic Theory (J. Wiley and Sons, New York)

Stoer J., Bulirsch R. 1980, Introduction to numerical analysis (Springer-Verlag, New-York) second ed., 1983

Zharkov V.N., Trubitsyn V.P. 1978, Physics of planetary interiors, ed. W.B. Hubbard (Pachart Press, Tucson)

Zharkov V.N., Gudkova T.V. 1992, In High pressure research: application to Earth and planetary sciences, eds. Y. Syono and M.H. Manghnani, TERRAPUB, Tokyo, 393–401